

CURRENT COLLECTION IN A FLOWING MAGNETOPLASMA

Nagendra Singh and B.I. Vashi

Department of Electrical and Computer Engineering and

Center for Space Plasma and Aeronomic Research

University of Alabama, Huntsville, AL 35803

ABSTRACT: Effects of plasma drift on the current collection by a long conducting cylinder in a magnetized plasma is studied by means of a 2 1/2 dimensional PIC code. It is found that for the drift velocity (\underline{V}_0) perpendicular to the magnetic field \underline{B}_0 , the electron current collected by a positive cylinder is considerably enhanced depending on the drift velocity. The distributions of plasma and the potential structure around the cylinder for several relative orientations between \underline{V}_0 and \underline{B} are presented along with the comparisons of current with and without the magnetic field. Simulations with the magnetic field in the simulation plane show that the potential structures around the cylinder are two-dimensional double layers with dimension (L_{\perp}) perpendicular to \underline{B} much smaller than the dimension (L_{\parallel}) parallel to \underline{B} . In fact, L_{\perp} is found to be approximately determined by the current limiting radius given by the Parker-Murphy model. However, it is found that the collected currents in the simulations are generally higher than those given by this model.

1. INTRODUCTION

The knowledge of current collection by conducting bodies in space plasma is relevant to numerous applications such as the operation of plasma probes, charge neutralization on space vehicles, working of the solar cell arrays and the operation of an

electrodynamic tether. Most theories dealing with this topic are limited to simple geometries and idealized plasma models. For reviews of the theoretical studies, the reader is referred to Whipple and Laframboise and Sonmor in this volume. These reviews show that there is a general lack of theoretical studies on current collection in a magnetized plasma when there is a relative drift between the magnetized plasma and the current collector. The purpose of this paper is to contribute to this area by means of computer simulations using a PIC code.

Our computer model is two dimensional; the axis of the cylinder is perpendicular to the plane of simulation. The magnetic field is oriented along the axis of the cylinder or in the simulation plane in different simulations, which bring out the effects of relative orientation between the magnetic field and the plasma drift on the sheath structure and the current collection properties. For the axial magnetic field, a simple-minded picture with radial electric fields indicates that the $\underline{E} \times \underline{B}$ drift will cause a magnetic insulation stopping any collection of electrons by the positive cylinder. Simulations show that this picture is not valid when there is a relative flow between the plasma and the cylinder; the potential structure is considerably modified so that the flowing electrons are focused onto the cylinder, making possible the collection of a relatively large electron current.

When the magnetic field is in the simulation plane, the potential structure is extended along the magnetic field and its transverse dimension is quite limited and it is found to be given by the current limiting radius calculated by Parker and Murphy [1] in a non-flowing plasma. We find that when the flow is perpendicular to the magnetic field, the electrons intercepted by the extended field-aligned potential structure are partially collected by the cylinder and the current is found to be considerably enhanced over the current predicted by the Parker-Murphy model [1]. However, for the flow parallel to the magnetic field, the current is seen to be limited in a fashion described by the above model. Since in the low earth orbit, the orbital velocity vector is at large oblique angles with respect to the geomagnetic field, a current enhancement is expected.

2. SIMULATION TECHNIQUE

The plasma flow past the cylinder is simulated as shown in Figure 1. The hatched area is the end view of the long conducting cylinder of radius r_s . In the rest frame of the cylinder, plasma flows along the positive x direction with the velocity V_0 . The flow is facilitated by imposing a dc convection electric field E_0 so that $V_0 = \underline{E}_0 \times \underline{B}/B^2$. The simulated plasma region is limited to $r \leq R_{\max}$ (Figure 1). At the initial time $t = 0$, the simulation region is a vacuum and the plasma flow for $t > 0$ is maintained by injecting charged particles at the rim of the simulation box ($r = R_{\max}$) over the angular region $\pi/2 \leq \theta \leq 3\pi/2$ (Figure 1). The average injection velocity of the charged particles is V_0 . At each time step a predetermined number (N_{inj}) of electron-ion pairs are injected to simulate a desired plasma flux. The plasma particles used in the simulations are like rods parallel to the axis of the cylinder [2]. The injected particles are chosen from Maxwellian

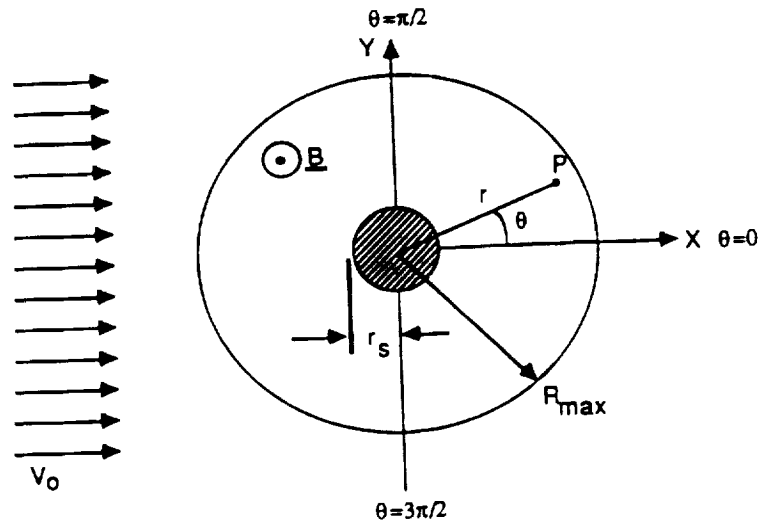


Figure 1. Geometry of the simulation. The conducting cylinder is shown by the hatched region. R_{\max} gives the radius of the simulation system. Plasma flows across the cylinder with a velocity \underline{V}_0 . The magnetic field is parallel to the axis of the cylinder.

distributions with electron temperature $T_e = T_0$ and ion temperature $T_i = 0$. The Y coordinates of the particles are chosen according to a uniform probability distribution. The X coordinates are first calculated by $X = (R_{\max}^2 - Y^2)^{1/2}$ and then further randomized by replacing X by $X + V\Delta t$ where V is the particle velocity randomly chosen from a Maxwellian distribution and Δt is the time step. Our injection technique is quite similar to that described by Aldrich [6].

The magnitude of charge (q_α), per unit length of such computer particles, is obtained by balancing the plasma flux into the simulation region at the injection boundary and the simulated flux due to the injection of the charge particles at each time step of duration Δt , giving

$$|q_\alpha| = 2 R_{\max} e N_0 V_0 \Delta t / N_{\text{inj}} \quad \text{C/m} \quad (1)$$

where N_0 is the ambient plasma density and e is the magnitude of the electron charge. The injection of equal numbers of electrons and ions insures that no net charge is injected into the system.

The temporal and spatial evolutions of the plasma and fields are calculated by the self-consistent solutions of the equations of motions [2] of all the charged particles and the Poisson equation for the electric potential ϕ . It is important to note that in our simulations, the electric field has two contributions as indicated by the following equation

$$\underline{E} = \underline{E}_0 + \underline{E}_1 \quad (2)$$

where \underline{E}_0 is the convection field and \underline{E}_1 is determined by the space charges and the bias potential on the cylinder. Since \underline{E}_0 is uniform in space, $\nabla \cdot \underline{E}_0 = 0$ and the divergence of (2) gives

$$\nabla \cdot \underline{E} = \nabla \cdot \underline{E}_1 = \rho / \epsilon_0 \quad (3)$$

where ρ is the electric charge density. Under the electrostatic approximation, $\underline{E}_1 = -\nabla\phi$ and (3) gives the Poisson equation

$$\nabla^2 \phi = -\rho / \epsilon_0 \quad (4)$$

The boundary conditions on the electric potential ϕ are $\phi(r = r_s, \theta) = \phi_0$ and $\phi(r = R_{\max}, \theta) = 0$, where ϕ_0 is the bias potential of the cylinder. The particles striking the cylinder and those leaving the system are assumed to be lost. However, the simulation system is maintained quasi-neutral at the 'global' scale. For this purpose, we compare the total numbers of electrons and ions in the entire system at each time step. The deficit charged particles, which are taken from a Maxwellian plasma reservoir are randomly distributed over the entire simulation system according to a uniform probability distribution.

The collected current (I) is calculated by counting the electrons and ions striking the cylinder during each time step,

$$I = \sum_{\alpha} q_{\alpha} \delta N_{\alpha} / \Delta t \quad (5)$$

where δN_{α} is their number, and q_{α} is given by (1). We note that although q_{α} depends on the numerical factors R_{\max} , N_{inj} and Δt ; the current I is found to be independent of them, if R_{\max} and N_{inj} are sufficiently large and Δt is sufficiently small. This was verified by carrying out simulations by varying these parameters.

3. NORMALIZATIONS AND DEFINITIONS

We discussed earlier that the charge on a computer particle is given by (1). If $q_{\alpha}/e = \eta$, the analogy between the real and computer particles requires that the masses m , effective temperatures T and density N satisfy the relations

$$m_{c\alpha} = \eta m_{r\alpha}, \quad T_{c\alpha} = \eta T_{r\alpha} \quad \text{and} \quad N_{c\alpha} = N_{r\alpha} / \eta \quad (6)$$

where the subscripts r and c refer to the real and computer particles, respectively. It is worth mentioning that the electron and ion Debye lengths and plasma frequencies are invariant under the scaling law described by (6) [4].

The results presented in this paper are based on simulations with the following ionospheric plasma parameters: ambient plasma density $N_0 = 10^{11} \text{m}^{-3}$, electron

temperature $T_e = 0.2$ eV, plasma debye length $\lambda_{do} \simeq 1$ cm, electron plasma frequency $\omega_{po} \simeq 1.8 \times 10^7$ rad/s, and the magnetic field $B_o = 0.3$ G. With the above ambient plasma parameters, the electron thermal current $J_r = N_o e V_{te} / \sqrt{2\pi} \simeq 1.2$ mA/m², where $V_{te} = (kT_o/m_e)^{1/2} \simeq 192$ km/s.

In order to simplify the equations and to generalize the applicability of their solutions to different situations with varying plasma and current-collector parameters, we use the following normalizations: potential $\tilde{\phi} = \phi/\phi_n$, $\phi_n = k_B T_e/e$; time $\tilde{t} = t\omega_{po}$; velocity $\tilde{V} = V/V_{te}$ and distance $\tilde{r} = r/\lambda_{do}$.

In view of the above normalizations the Poisson equation (4) can be written as

$$\frac{\partial^2 \tilde{\phi}}{\partial \tilde{r}^2} + \frac{1}{\tilde{r}} \frac{\partial \tilde{\phi}}{\partial \tilde{r}} + \frac{1}{\tilde{r}^2} \frac{\partial^2 \tilde{\phi}}{\partial \tilde{\theta}^2} = - \frac{\lambda_{do}^2}{\phi_n} (qn_{ic} - qn_{ec}) \quad (7)$$

where qn_{ic} and qn_{ec} are the charge per unit volume associated with the computer ions and electrons, respectively. It is assumed that both types of particles have the same magnitude of charge, i.e., $q_e = q_i = q$, as given by (1). These charge densities (qn_{ic} and qn_{ec}) are determined by calculating the number of computer particles at each grid point by the area sharing method [2] and dividing it by the effective volume of a cell. This volume is given by $r_j \Delta \theta \Delta r \Delta z$, where r_j is the radial distance of a grid point, Δr and $\Delta \theta$ are the radial and angular grid spacings, respectively and Δz is the length along the axial direction. With these definitions and equation (1), the normalized Poisson equation takes the form

$$\frac{\partial^2 \tilde{\phi}}{\partial \tilde{r}^2} + \frac{1}{\tilde{r}} \frac{\partial \tilde{\phi}}{\partial \tilde{r}} + \frac{1}{\tilde{r}^2} \frac{\partial \tilde{\phi}}{\partial \tilde{\theta}^2} = - 2\tilde{R}_{max} \tilde{V}_o \Delta \tilde{t} (\Delta n_{ic} - \Delta n_{ec}) / \tilde{r}_j \Delta \tilde{r} \Delta \tilde{\theta} N_{inj} \quad (8)$$

where Δn_{ic} and Δn_{ec} are the number of computer ions and electrons shared on a grid point ($j\Delta r, i\Delta \theta$). The above equation is solved by employing FFT in θ and triadiagonal method in r .

The numerical results presented below are based on the following numerical parameters: $R_{max} = 140\lambda_{do} \simeq 1.4$ m, $r_s = 10\lambda_{do} \simeq 0.1$ m, $\Delta \tilde{t} = 0.2$, $\Delta \tilde{r} = 1$, $\Delta \theta = 10^\circ$ and the normalized flow velocity $\tilde{V}_o = V_o/V_{te}$ is varied. The simulations are carried out with H^+ plasma for which $m_i/m_e = 1836$. We note that in our simulation electron

cyclotron period $\tau_{ce} \approx 18 \omega_{po}^{-1}$ while the ion cyclotron period $\tau_{ci} \approx (m_i/m_e) \tau_{ce}$. Thus, for the time scales in the simulations, electrons are magnetized, while ions behave as unmagnetized charged particles.

4. NUMERICAL RESULTS

In the following discussion we first present results for $B = 0$, which are later used for the purpose of comparisons with the results for non-zero magnetic fields with different orientations.

4.1 Simulations with $B = 0$

We recall that the simulation begins with no initial plasma in the system. The simulation plasma builds up in the system in response to the injection of particles as described above in Section 2. In the simulation described in this subsection $\tilde{\phi}_0 = 100$ and $\tilde{V}_0 = 0.3$. Figures 2 and 3 show the evolution of the plasma; in Figure 2 the contours of constant density of ions are shown at some selected times. The minimum density contour is $\tilde{n} = 0.1$ and the density interval between the contours is $\Delta\tilde{n} = 0.3$. The electron density shows nearly the same evolution as the ions. After about $\tilde{t} = 550$, a quasi-steady state is reached in the plasma distribution.

The distribution of the computer particles in the $r-\theta$ plane are shown in Figure 3, each dot in the panels of this figure represents a particle. The left-hand panels show electrons while the right-hand ones show ions. Note the formation of a distinct wake behind the cylinder (also see Figure 2). Another noteworthy feature of Figures 2 and 3 is that a bow structure forms in the ram direction; in this structure the density is generally enhanced. We also see from Figure 3 that ions are not able to reach the cylinder because the kinetic energy of the ions ($1/2 m_i V_0^2 = 82.6 \text{ kT}_0$) associated with the plasma drift is smaller than the potential energy $e\phi_0 = 100 \text{ kT}_0$, where ϕ_0 is the bias voltage on the cylinder. Outside the wake region, the plasma density $\tilde{n} = 1$, indicating a uniform plasma flow in the ram direction away from the bow structure.

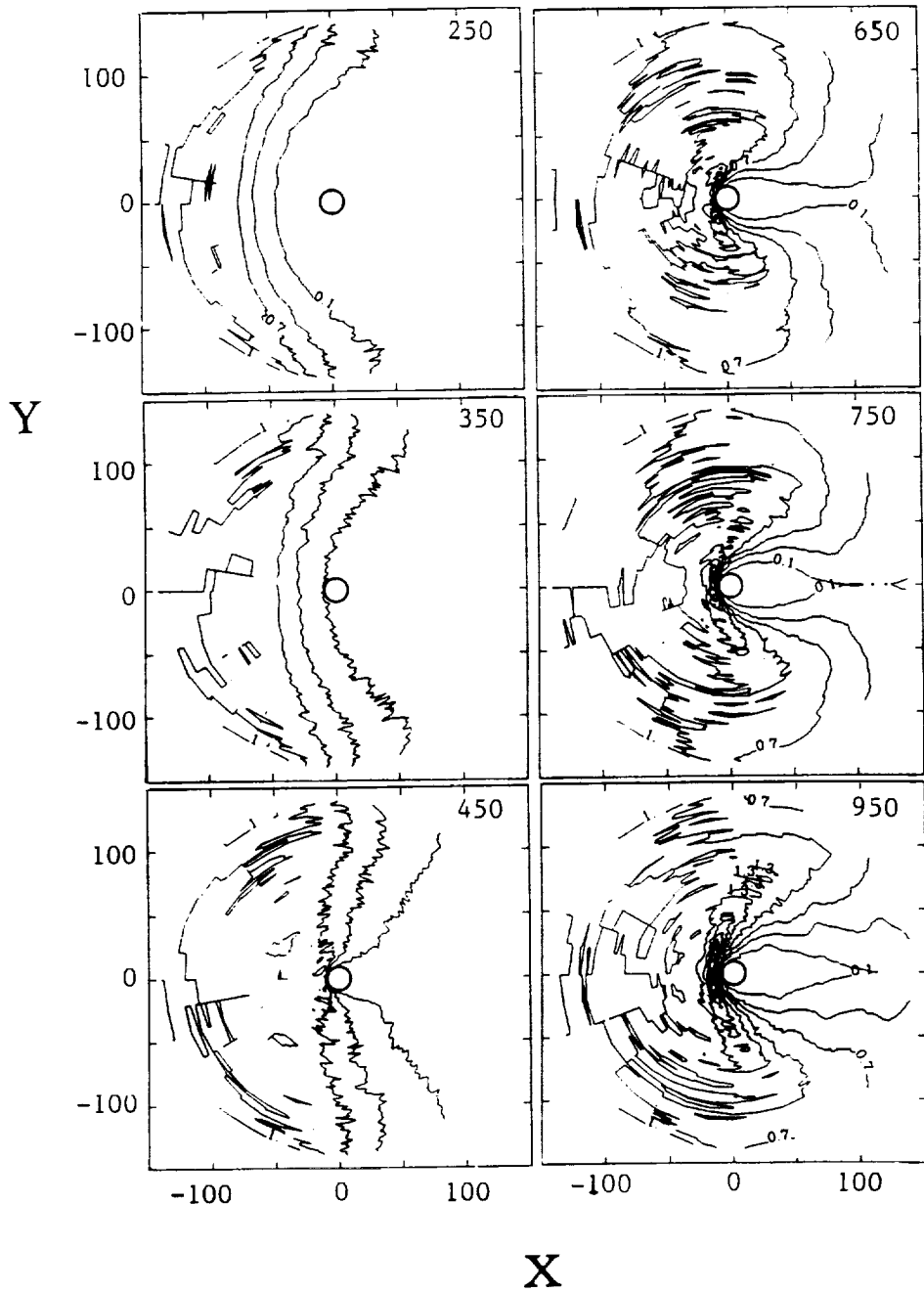


Figure 2. Evolution of the plasma inside the simulation region. Contours of constant densities are shown with a contour spacing of $\Delta \tilde{n}_i \approx 0.3$. Note that the plasma distribution attains a quasi-steady state after about $\tilde{t} = 600$. $\tilde{\phi}_0 = 100$.

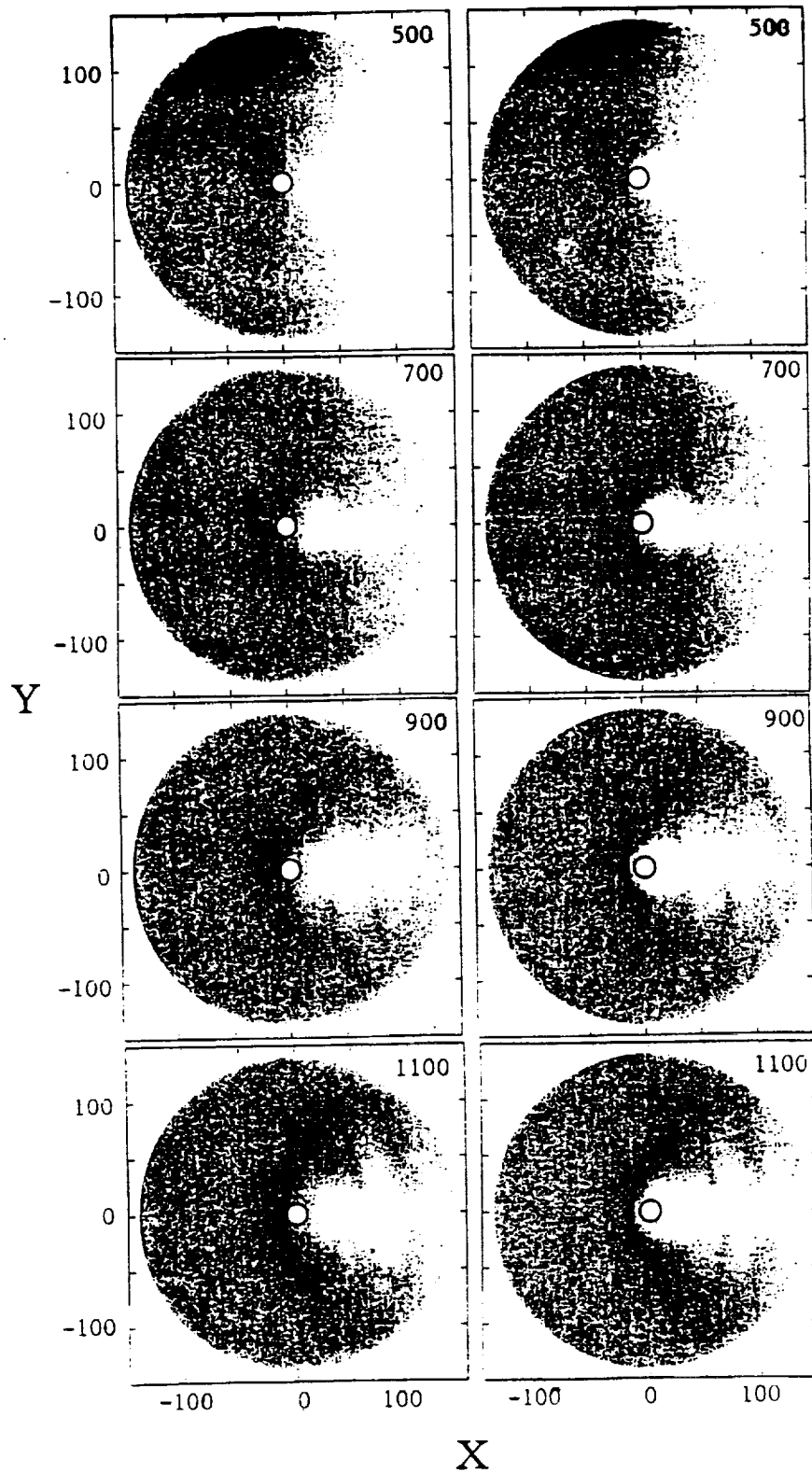


Figure 3. Evolution of plasma is shown by showing the distribution of (a) electrons and (b) ions in the $r-\theta$ plane. Each dot in this figure represents a computer particle. $\bar{\phi}_0 = 100$, $B = 0$, $\bar{V}_0 = 0.3$.

The evolution of the potential distribution around the cylinder is shown in Figure 4, which gives the equipotential surfaces at some selected times. The contour levels are $\Delta\tilde{\phi} = 5$ apart. This figure shows that after about $\tilde{t} = 500$, the sheath structure reaches a quasi-steady state. In the wake region the potential is generally negative.

In response to the evolution of the plasma and potential around the cylinder, the collected current evolves as shown in Figure 5. The current reaches a quasi-steady state after about $\tilde{t} = 500$, in agreement with the evolutions of the density and the plasma potential. After this time, the plasma and the potential are still undergoing some changes, especially in the wake region, but they seem to have negligible effect on the current collection. The time-average current for $B = 0$ in the quasi-steady state ($\tilde{t} > 500$) is about $I \approx 18$ mA.

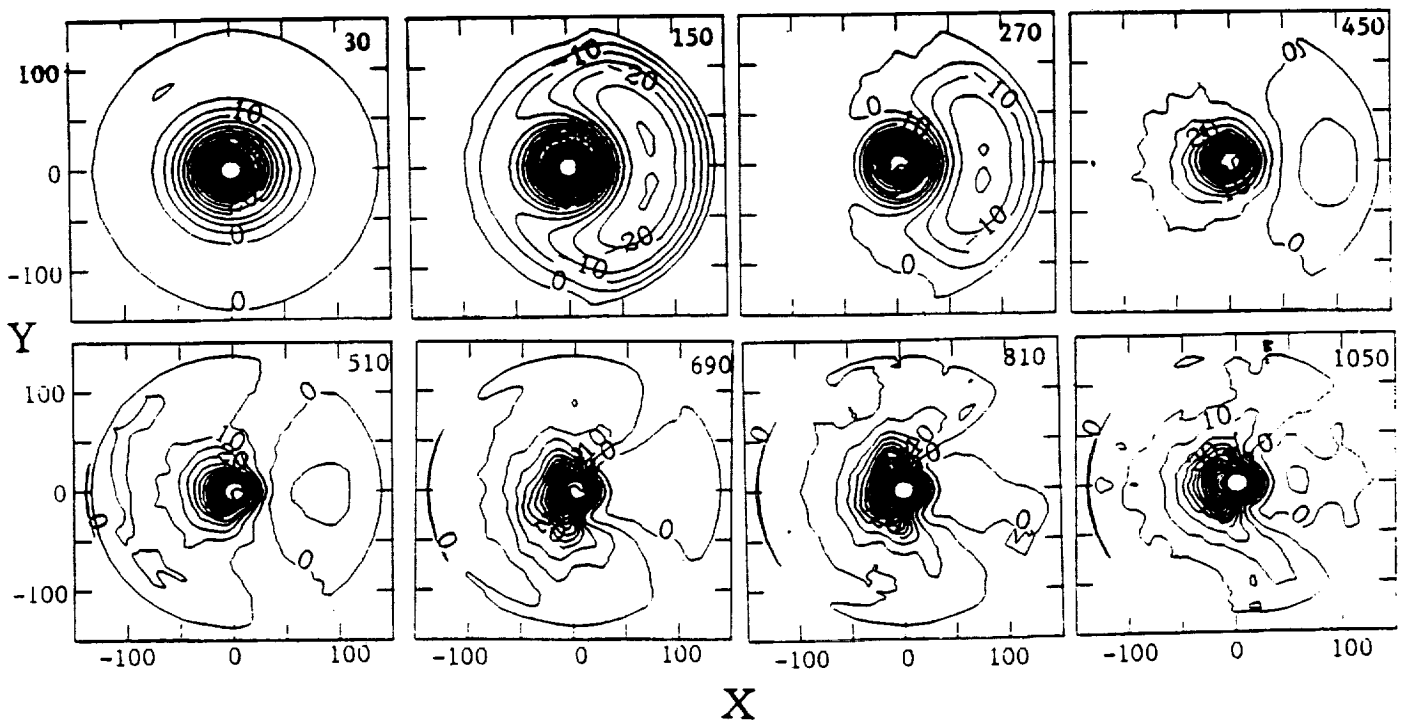


Figure 4. Evolution of the equipotential surfaces around the cylinder. Note that after about $\tilde{t} = 600$, the equipotential surfaces attain a quasi-steady state. The equipotential contours are $\Delta\tilde{\phi} = 5$ apart. $\tilde{\phi}_0 = 100$, $B = 0$, $\tilde{V}_0 = 0.3$

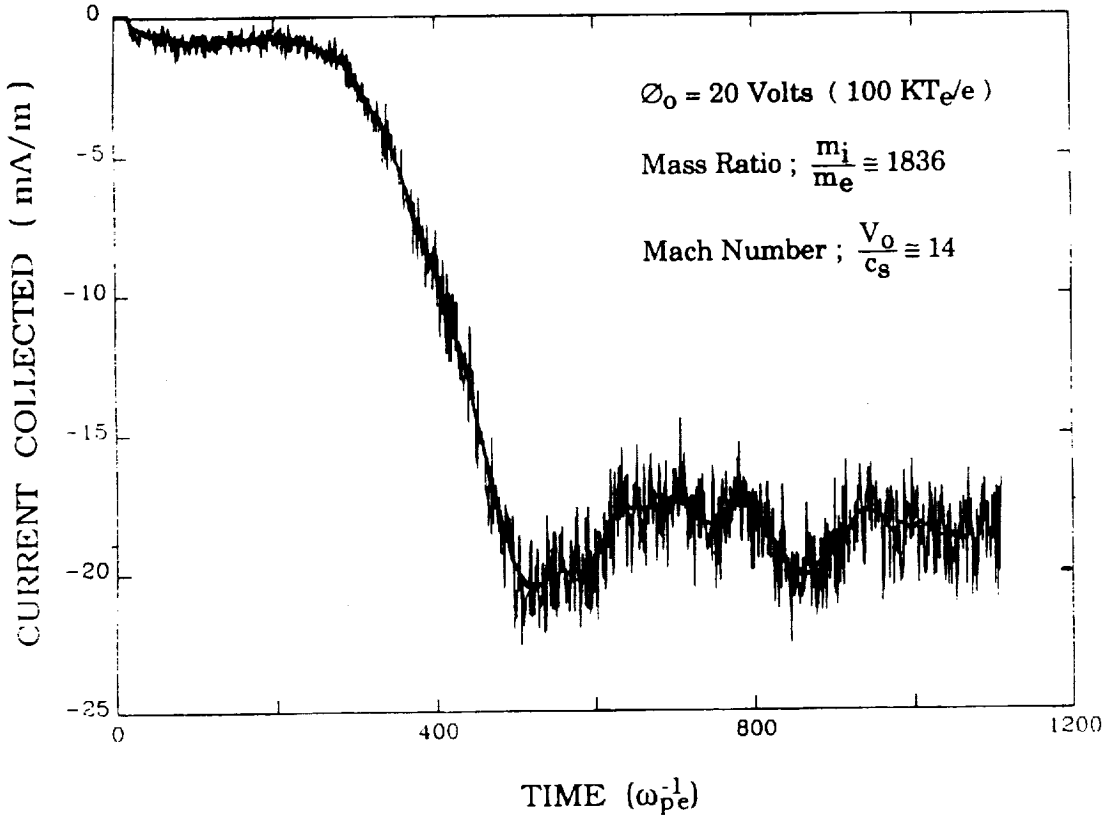


Figure 5. Temporal evolution of the current collected by the cylinder. The thick line curve shows the time average current when fast oscillations are averaged out. Note that the current attains a quasi-steady state when about $t \geq 600$.
 $\bar{\phi}_0 = 100, B = 0, \bar{V}_0 = 0.3$

The simulations with $B = 0$ were carried out for several bias potentials. Figure 6 shows the V - I characteristics of the cylinder. It is found that $I \propto \phi_0^{1/2}$, which is in agreement with the orbit-limited current collected by a cylinder (e.g. see Chen [5]). However, the proportionality constant is found to be given by

$$I \simeq 1.8 (e\phi_0/kT_e)^{1/2} \text{ mA/m},$$

which is found to be by a factor of two larger than that for $V_0 = 0$. It is expected that in the limit $V_0 = 0$, the simulations must yield the current as predicted by the orbit-limited current. However, the simulation runs with very small drift velocities take too long to complete and so far we have not carried out such simulations.

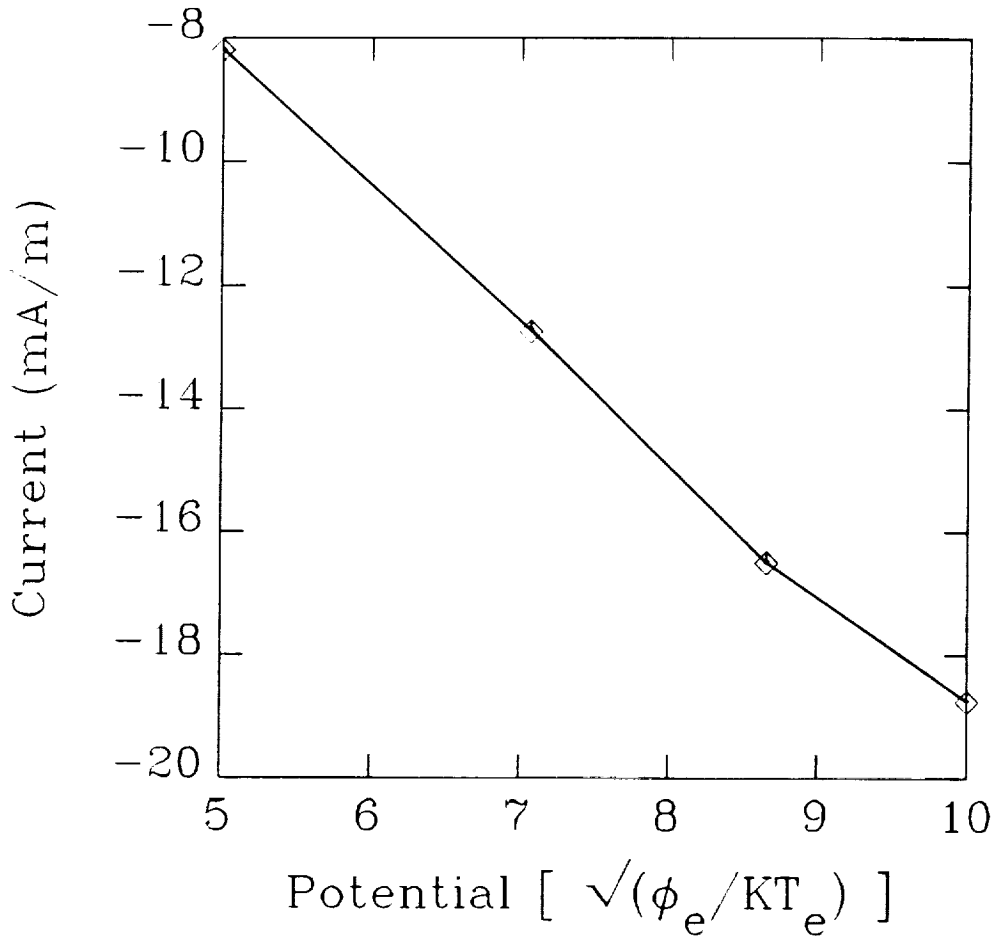


Figure 6. I-V characteristic of the cylinder. Note that the horizontal axis is $\phi_0^{1/2}$. The current variation shows the linear relation $I \propto \phi_0^{1/2}$. $\tilde{V}_0 = 0.3$, $B = 0$.

4.2 Simulation with $B = B_z = 0.3$ G and $\tilde{\phi}_0 = 100$

We do not show the temporal evolution of the plasma and potential here, instead we just present here the quasi-steady state distribution of the plasma and potential around the cylinder. The top two panels of Figure 7 show the contours of constant ion and electron densities. The corresponding distributions of the particles in the r - θ plane are shown by the two middle panels. The bottom single panel shows the distribution of potential; equipotential surfaces at intervals of $\Delta\tilde{\phi} = 5$ are shown. It is worth pointing out that the plasma and potential distributions for $B_z = 0.3$ Gauss is quite different from those for $B = 0$. In the former case ($B_z = 0.3$ Gauss), the equipotentials show a multicell convection pattern [6]. The fan-shaped structure extending below the cylinder is the

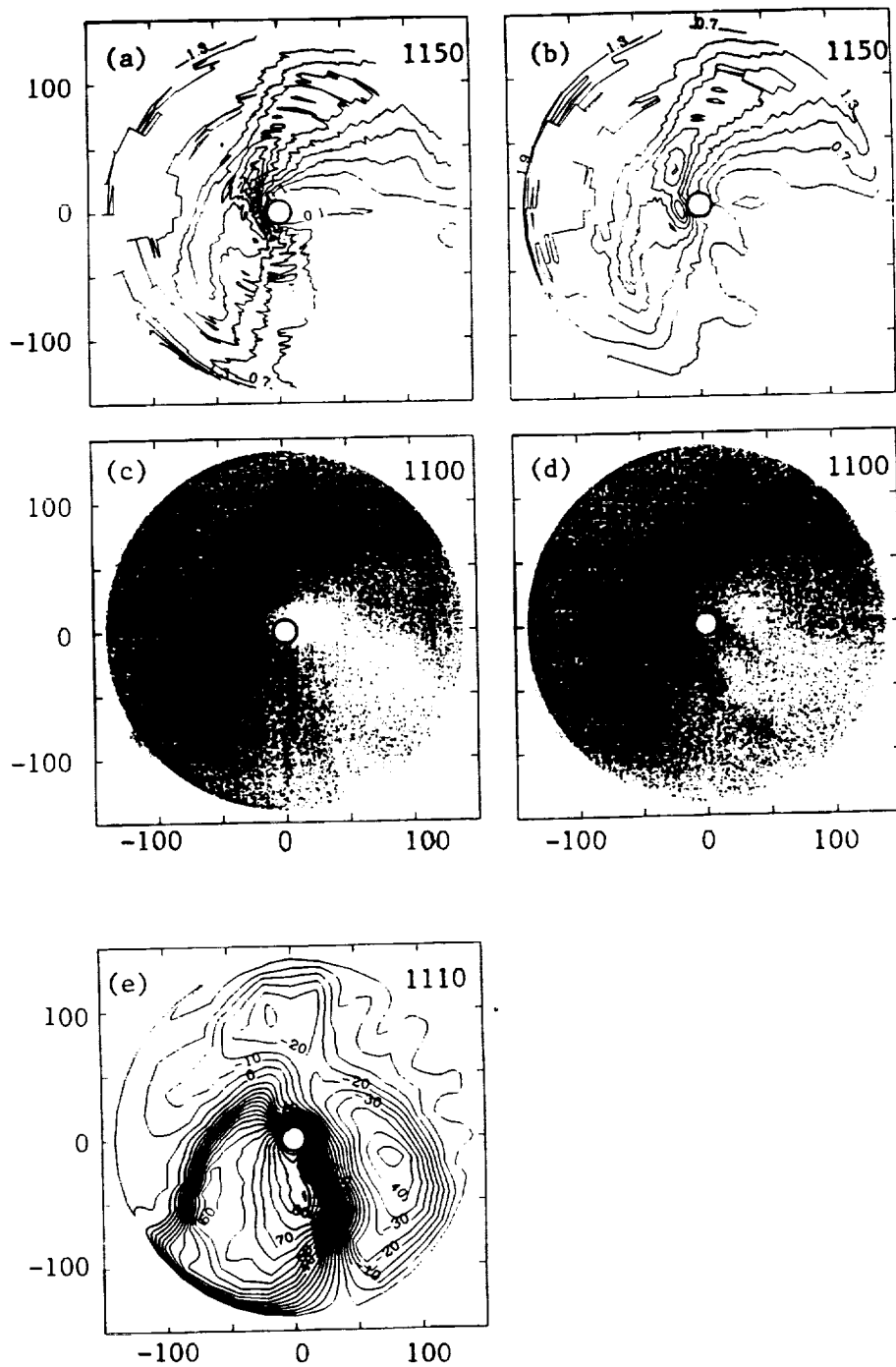


Figure 7. Quasi-steady state feature of the plasma (a) Ion density distribution, (b) electron density distribution. The contour levels in (a) and (b) are $\Delta \bar{n} = 0.3$ apart. (c) spatial distribution of ions, (d) spatial distribution of electrons, (e) distribution of potential; equipotential surfaces are $\Delta \bar{\phi} = 5$ apart. $\bar{\phi}_0 = 100$, $B = 0$, $\bar{V}_0 = 0.3$.

consequence of the stagnation of the plasma flow below the cylinder due to the opposition to the flow by the $\underline{E} \times \underline{B}$ drift in the initial radial electric field [6]. The fan-shaped equipotentials cause electrons to circulate around the cylinder due to the $\underline{E} \times \underline{B}$ drift. The electron flow coming from the left is caught in this convection cell and focused on to the cylinder as shown by the crowded equipotentials immediately on the top of the cylinder. This circulation of the flowing electrons facilitates their collection by the cylinder.

The temporal evolution of the current collected by the cylinder with the axial field B_z is shown in Figure 8. The current is seen to reach a quasi-steady state at about $\bar{t} \approx 700$, after which its average value $I \approx 14$ mA/m, which is only slightly lower than 18 mA/m for $B = 0$. The simulation with the axial magnetic field shows that the magnetic insulation due to $\underline{E} \times \underline{B}$ drift in the initial radial electric field is destroyed due to the considerable modification of the potential distribution caused by the plasma flow [6].

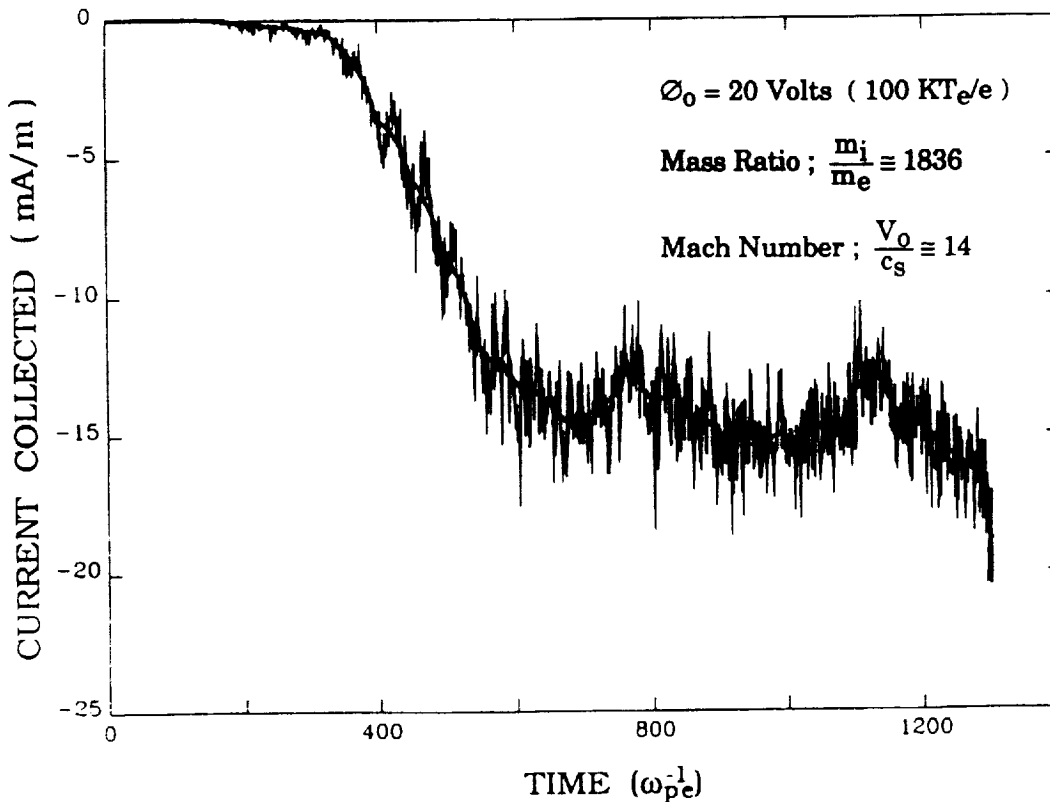


Figure 8. Temporal evolution of the current for $B_z = 0.3$ G, $\bar{\phi}_0 = 100$ and $\bar{V}_0 = 0.3$.

4.3 Simulation with $B = B_y = 0.3$ Gauss, and $\tilde{\phi}_0 = 50$

Note that in this case the magnetic field is in the plane of the simulation. This allows us to study the B field-aligned potential structures. The quasi-steady state distributions of the plasma and potentials are shown in Figure 9. The top two panels show the contours of the ion and electron densities. The corresponding distributions of ions and electrons in the r - θ plane are shown in the middle panels. The wake structure is clearly seen from these panels. In the ram direction the plasma is generally uniform with the normalized density $\tilde{n} = 1$. The bottom panels show the equipotential surfaces from simulation with $\tilde{\phi}_0 = 50$ (left) and $\tilde{\phi}_0 = 25$ (right). These bottom panels show that the potential distributions are extended along the magnetic field. When $\tilde{\phi}_0 = 50$, the potential structure is seen to extend all the way to the boundary of the simulation plasma. In order to examine the effect of the boundary the simulation was repeated by lowering $\tilde{\phi}_0$ to 25 and increasing the size of the system from $\tilde{R}_{\max} = 140$ to 185. The result is shown in the bottom right-hand panel. It is seen that potential structure is now nearly fully accommodated in the simulation region.

It is interesting to examine the size (L_{\perp}) of the potential structure transverse to the magnetic field. Figure 10 shows the radial distribution of the potentials for $\tilde{\phi}_0 = 50$ and 25 in the ram direction ($\theta = 180^\circ$). It is seen that the potential structure becomes narrower with increasing ϕ_0 . The radial distances at which $\phi = 0$ for the above bias voltages are given by

$$L_{\perp} \simeq 25 \lambda_d, \quad \tilde{\phi}_0 = 25 \quad (9a)$$

$$L_{\perp} \simeq 31 \lambda_d, \quad \tilde{\phi}_0 = 50 \quad (9b)$$

Parker and Murphy [1] have considered the collection of electrons by a positive sphere. Using conservation of energy and angular momentum, they have shown that in the case of non-flowing plasma, the electrons which are possibly collected by the sphere, are confined in a cylinder of radius r_0 as shown in Figure 11, where r_0 is given by

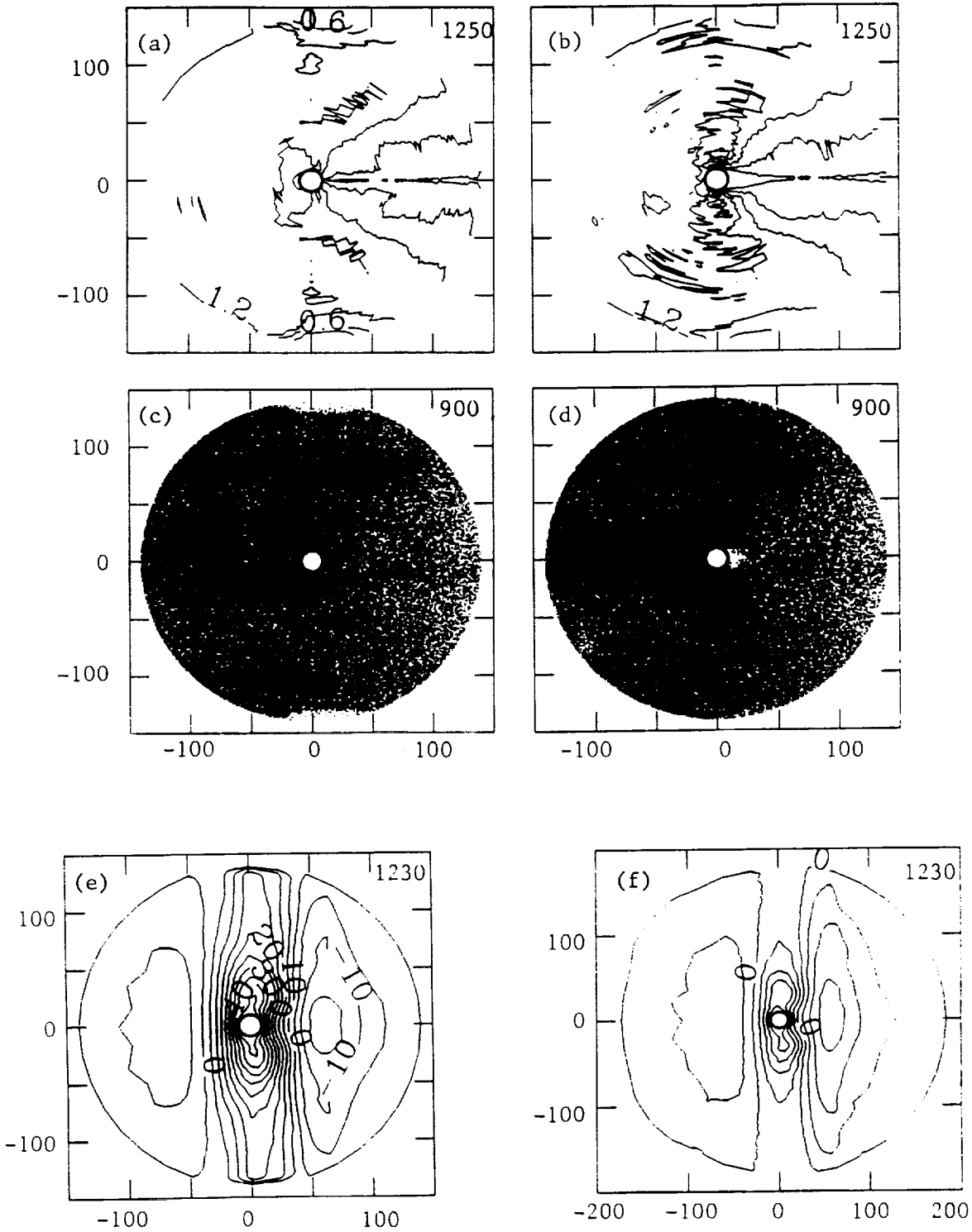


Figure 9. Quasi-steady state distributions of (a) electron density, (b) ion density, (c) electrons, (d) ions, (e) potential for $\tilde{\phi}_0 = 50$, $\tilde{V}_0 = 0.3$, $B = B_y = 0.3$ Gauss, and (f) potential distribution for $\tilde{\phi}_0 = 25$, $\tilde{V}_0 = 0.3$, $B = B_y = 0.3$ Gauss in a simulation with larger system size.

$$r_0 = \left[1 + \frac{2\rho_{e\phi}}{a} \right]^{1/2} a$$

$$\approx \sqrt{2 \rho_{e\phi} a}, \quad \rho_{e\phi} \gg a \quad (10)$$

where $\rho_{e\phi}$ is the electron Larmor radius with the electron energy $e\phi_0$. It is interesting to note that the value of L_{\perp} estimated above for $\tilde{\phi}_0 = 25$ and 50 are quite accurately given by (10), with a as the radius of the cylinder.

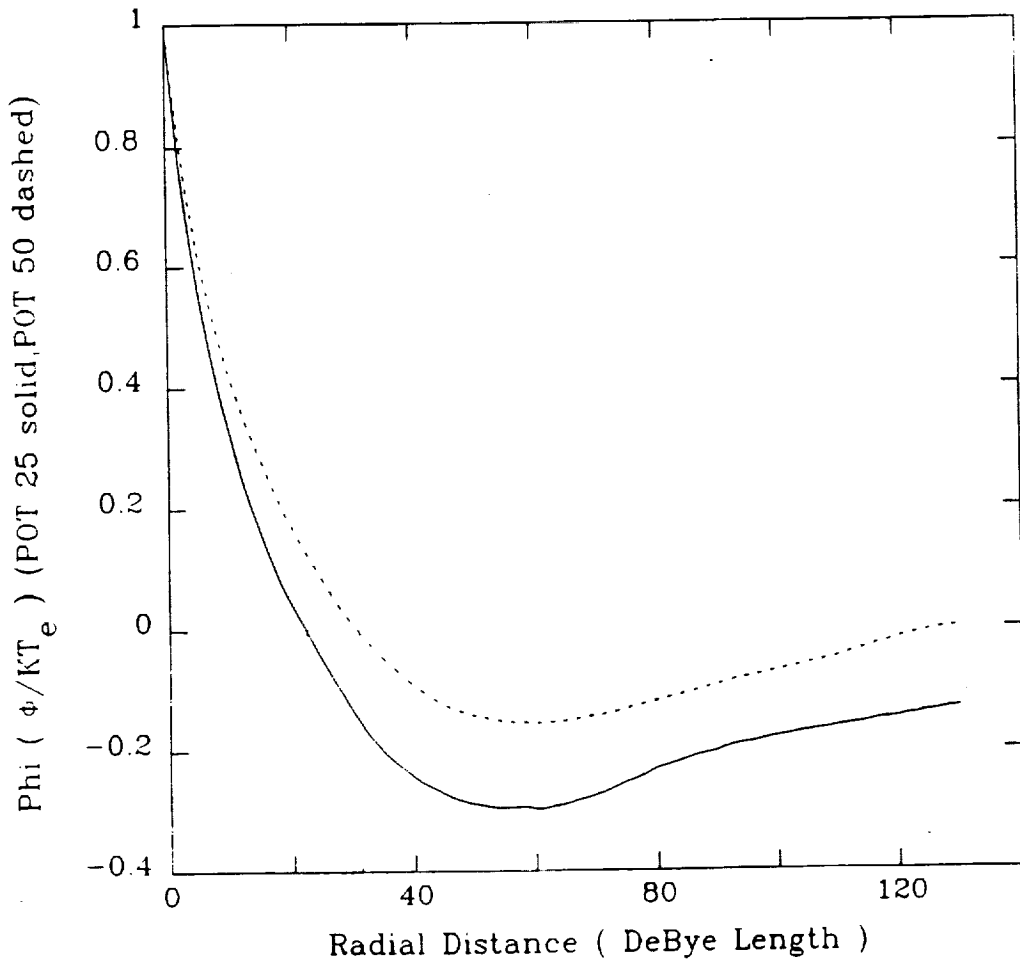


Figure 10 Radial distributions of potential for $\tilde{\phi}_0 = 50$ and 25 in the ram direction ($\theta = 180^\circ$). $B = B_y = 0.3$ Gauss. $\tilde{V}_0 = 0.3$.

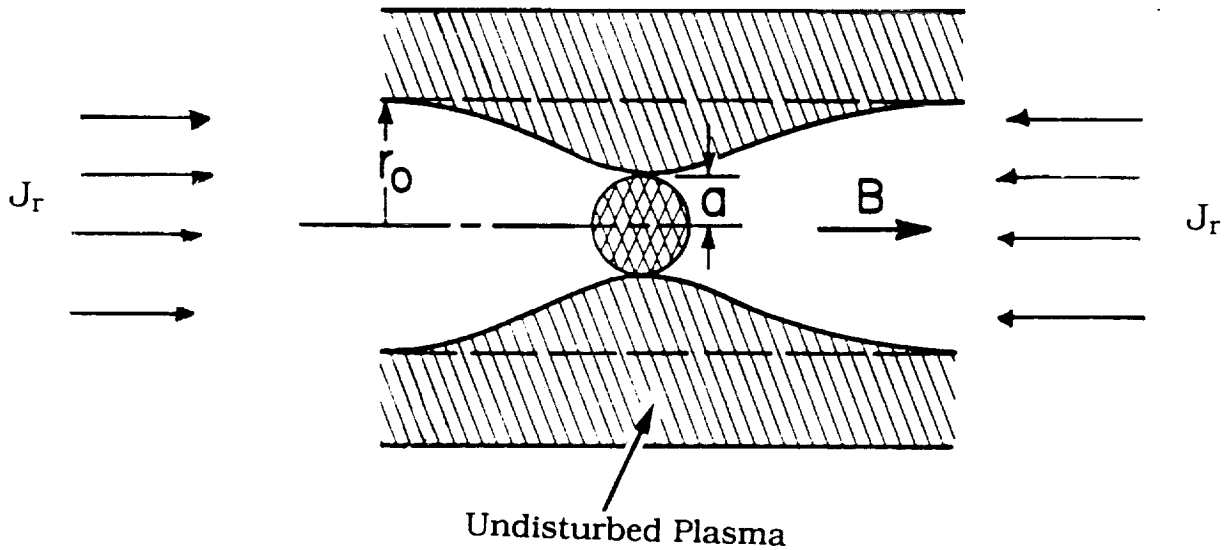


Figure 11 Geometry of the Parker–Murphy model for the current limitation. Electrons contained inside the cylindrical volume of radius V_0 are possibly collected by the electrode at a positive potential.

According to the Parker–Murphy model the current collected by the spherical electrode in a non–drifting plasma is simply the electron flux intercepted by the cylinder of radius r_0 (Figure 11):

$$I_{PM} = 2\pi r_0^2 J_r \quad (11)$$

where J_r is the electron thermal current given by $J_r = N_0 eV_{te}/\sqrt{2\pi}$. In the present situation, J_r is associated with the thermal motion along the y direction parallel to B_y .

We find that for the flow in a direction transverse to the extended potential structure, the current is considerably enhanced. If the current was collected primarily through the two ends of the potential structures (Figures 9e and 9f), the total electron current collected by the cylinder is given by

$$I_{PM} = 2 \times 2r_0 J_r \quad \text{A/m} \quad (12)$$

which is only about 1.2 mA/m for $\tilde{\phi}_0 = 25$. Our simulation shows a considerably larger collection of electron current. Figure 12 shows the evolution of the current collected by the

cylinder when $\phi_0 = 25$; in the quasi-steady state the current is about 7.5 mA/m, which is found to be close to the current collected without the ambient magnetic field with the same drift velocity $\tilde{V}_0 = 0.3$ (Figure 6). The excess current (~ 6.3 mA/m) is interpreted in terms of the interception of the electron flow by the extended potential structure along the magnetic field.

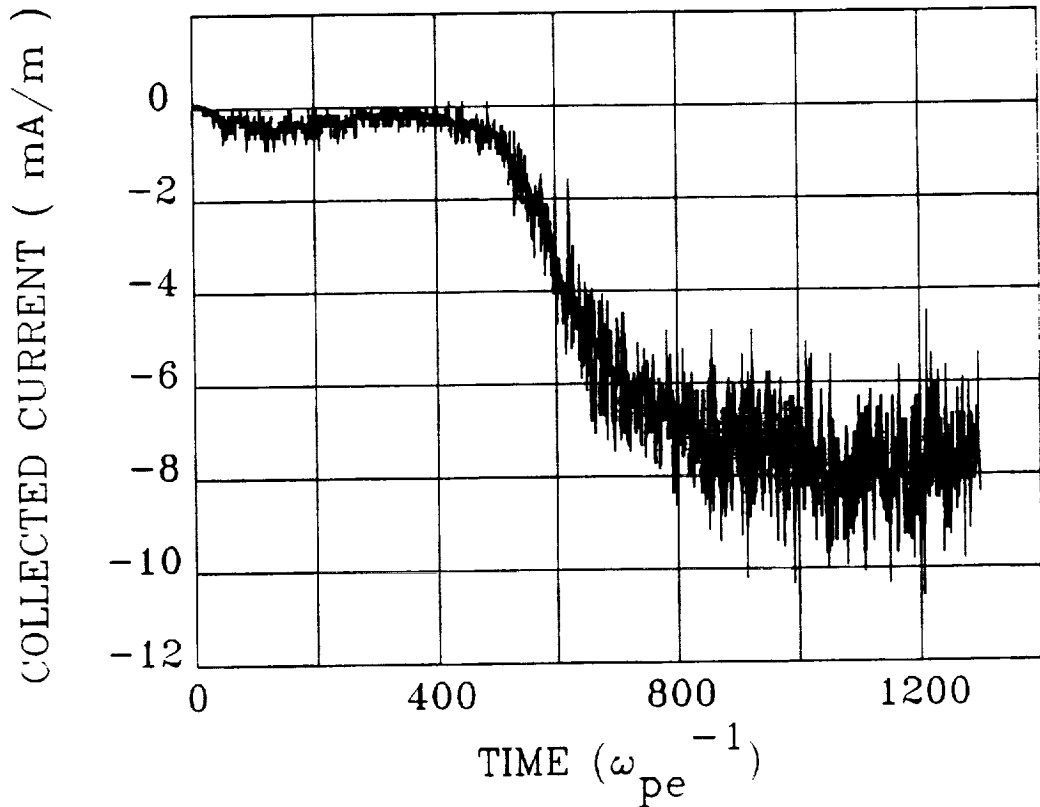


Figure 12 Temporal evolution of the current for $B = B_y = 0.3$ Gauss, $\tilde{V}_0 = 0.3$, $\tilde{\phi}_0 = 25$.

4.4 Simulation with $B = a_x B_0$

In order to examine the effects of relative orientation of the drift velocity with respect to the ambient magnetic field \underline{B}_0 in the simulation plane, we carried out another simulation with $V_0 \parallel B_0$. The potential structure for this case in the quasi-steady state is

shown in Figure 13. It is seen that now the potential structure is extended along x , the direction of the B field. Its transverse dimension L_{\perp} is again found to be limited according to (10), which gives the current limiting Parker–Murphy radius as a function of the bias voltage ϕ_0 . The temporal evolution of the collected current for $\underline{B} = \hat{a}_x B_0$ is shown in Figure 14a. For the purpose of comparison, the current with B_y is plotted in Figure 14b for the same value of $\tilde{\phi}_0 = 50$. Note the different vertical scales in Figures 14a and 14b. It is seen that for the flow along \underline{B} , the current is significantly reduced compared to the case with flow transverse to B . As noted earlier, in the later case the interception of the flow by the elongated potential structure enhances the current.

It is instructive to quantitatively compare the current from the Parker–Murphy model with that from the simulation with B_x . We already saw that the former current is

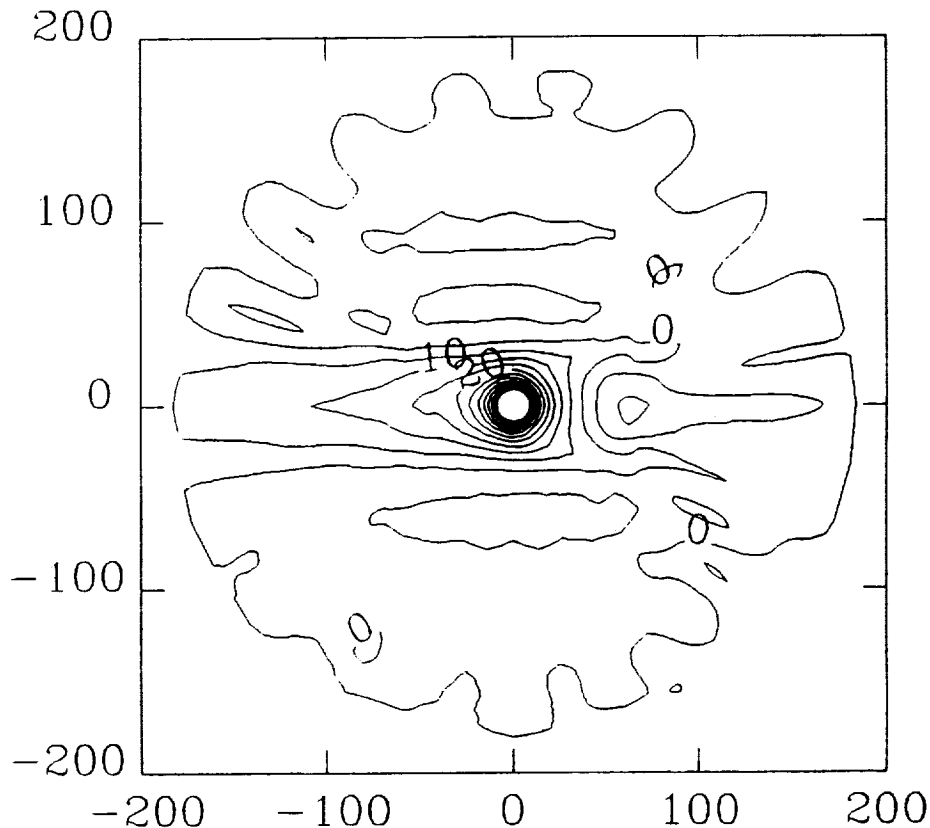


Figure 13 Quasi-steady state potential distribution for $B = B_x = 0.3$ Gauss, $\tilde{V}_0 = 0.3$, $\tilde{\phi}_0 = 50$.

given by (12). However, a few observations must be made while using this expression in the present case. The flow along the magnetic field makes the potential structure asymmetric with respect to $x = 0$ because of the formation of the wake behind the cylinder, making the first factor of 2 in (12) inaccurate. The use of this factor will give an overestimate. Furthermore, J_r in (12) must be replaced by a modified current density due to the plasma flow; for the flow velocity $V_o = 0.3 V_{te}$, this modified current density $J_e = 1.44 J_r$. With these considerations, (12) gives $I_{PM} < 2.2$ mA/m. Figure 14 shows that the time average current is about 3.5 mA/m, which is at least 60% larger than the current predicted from the Parker–Murphy model. The enhancement in the current suggests the transport of electrons across the magnetic field line. The exact mechanism for the cross–field electron transport has not been identified from the simulations. However, cross–field diffusion due to the fluctuations in the field need to be examined [7].

5. CONCLUSIONS AND DISCUSSION

The main conclusions of this paper are as follows:

- (i) When the relative plasma flow is transverse to the magnetic field, the current collected by a positive electrode can be considerably enhanced depending on the relative drift velocity.
- (ii) For the flow along the magnetic field, the current is limited as predicted by the Parker–Murphy model [1].
- (iii) Simulations with \underline{B} in the simulation plane show that the magnetic field–aligned potential structure is like a double layer with dimensions transverse to the magnetic field determined by the limiting radius given by the Parker–Murphy model [1], but it is extended along the field line.
- (iv) Simulation with the axial magnetic field shows that the potential structure represents a multi–cell convection pattern. The fan–shaped cell is seen to focus the electron flow on to the cylinder thus destroying the magnetic insulation effect.

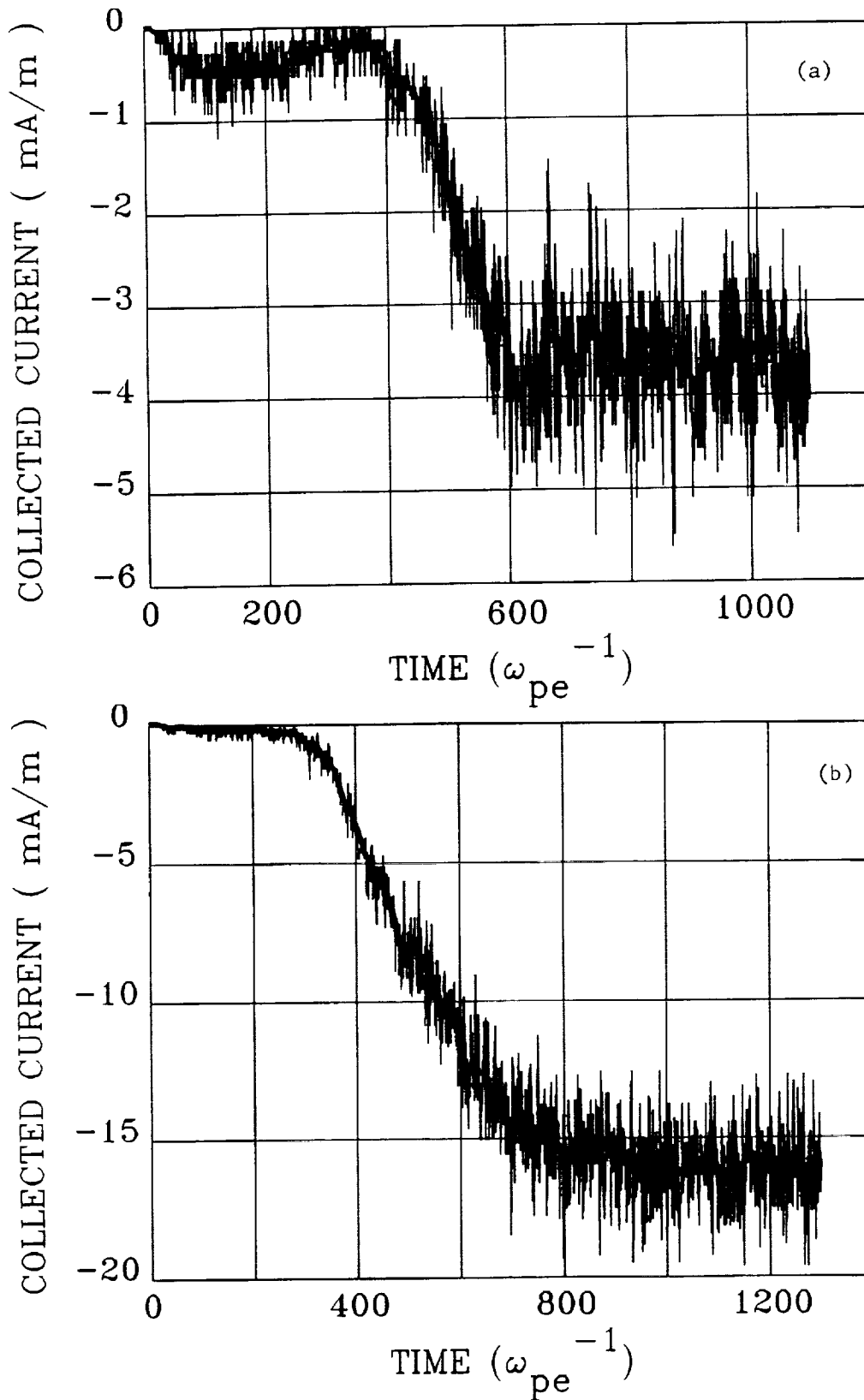


Figure 14 Temporal evolution of the current for (a) $B = B_x = 0.3$ Gauss, $\tilde{V}_0 = 0.3$, $\tilde{\phi}_0 = 50$. (b) $B = B_y = 0.3$ Gauss, $\tilde{V}_0 = 0.3$, $\tilde{\phi}_0 = 50$.

(v) In the low earth orbit, the orbital motion is nearly perpendicular to the magnetic field, and the relative flow velocity $V_o \simeq 8$ km/s, which can considerably enhance the current collection.

* In a real situation with an arbitrary orientation between \underline{B}_o and \underline{V}_o , the potential structure will be the combinations of the structures shown in this paper.

Recently Myers et al. [8] have demonstrated that the measured currents in a rocket experiment agree well with the predictions from the Parker–Murphy model [1]. Raitt et. al [this volume] have carried out a similar comparison. Since in the rocket experiments the relative drift velocities are only a few hundred meters per second, the current enhancement due to the relative drift is not expected to be significant.

In our present simulations plasma flows while the electrode is standing. In space the electrode cuts across the magnetic field lines. This raises some question about the dynamical effects. We note that in the simulations starting with an initial vacuum state, the quasi–equilibrium is reached quite quickly in a time of about $500\omega_{po}^{-1} \simeq 30 \mu s$. In real situations of space the quasi–equilibrium condition are expected to reach in a considerably shorter time. On the other hand, the contact time of a current collector with a magnetic flux tube depends on its sheath size. If we use the sheath size as given by (10) for large electrode voltages, the contact time τ_c can be estimated by

$$\tau_c = 2\sqrt{\rho_e \phi_o^2} / V_o$$

Using typical parameters ($\phi_o = 100$ V, $a = 1$ m, $B = 0.3$ G and $V_o = 8$ km/s) it is found that $\tau_c \geq 250 \mu s$. Comparing this time with the sheath establishment time of the order of a few tens of microseconds, it is inferred that the quasi–equilibrium conditions for the potential structure and the current collection as found from the simulations are likely to be maintained for a current collecting electrode in the low earth orbit.

6. ACKNOWLEDGEMENT

This work was supported by NASA Grant NAGW–1562. The simulation code was developed under a grant from the CRAY Research Inc.

REFERENCES

- [1] Parker, L.W. and B.L. Murphy, Potential Buildup of an Electron-Emitting Ionospheric Satellite, *J. Geophys. Res.*, 72, 1631, 1967.
- [2] Morse, R.L., Multidimensional Plasma Simulations by Particle-in-Code Methods, in *Computational Physics*, edited by Alder, Fernbach and Rotinberg, 9, 213, Academic Press, New York, Vol. 9, 213, 1970.
- [3] Aldrich, C.H., Particle Code Simulations Using Injected Particles, in *Space Plasma Simulations*, ed. by M. Ashour-Abdalla and D.A. Dalton, D. Riedel Publ. Comp., Boston, p. 131, 1985.
- [4] Thiemann, H., N. Singh, R.W. Schunk and R. Grard, Numerical Simulation of Spacecraft Charging by Impact-Produced Plasmas During a Cometary Flyby, *J. Geophys. Res.*, 91, 2989, 1986.
- [5] Chen, F.F., *Plasma Diagnostic Techniques*, edited by R.H. Huddlestone and S.L. Leonard, Chapt. 4, Academic Press, New York, 1964.
- [6] Singh, N. and B.I. Vashi, Current Collection by a Long Conducting Cylinder in a Flowing Plasma, AIAA 90-0724, Jan. 8-11, 1990/Reno, Nevada.
- [7] Linson, L.M., Current-Voltage Characteristics of an Electron-Emitting Satellite in the Ionosphere, *J. Geophys. Res.*, 74, 2368, 1969.
- [8] Myers, M.B., W.J. Raitt, B.E. Gilchrist, P.M. Banks, T. Neubert, P.R. Williamson and S. Susaki, A Comparison of Current-Voltage Relationships of Collectors in the Earth's Ionosphere with and without Electron Beam Emission, *Geophys. Res. Lett.*, 16, 365, 1989.